Applied Water Science (2023) 13:215
https://doi.org/10.1007/s13201-023-02021-1

ORIGINAL ARTICLE

Experimental study on parametric configurations of artificially downwelling aerations in stratified water

Xiaoqing Tian[1,2] · Zhenlin Wang[1] · Baofeng Zhang[3] · Ran Zeng[1] · Jiyong Wang[4] · Muk Chen Ong[5] · Junyi Yang[1]

Received: 11 May 2023 / Accepted: 9 October 2023 / Published online: 26 October 2023

Abstract

Downwelling aeration has become a widely applied approach to cope with the water eutrophication in stratified reservoirs, rivers and lakes. The aeration parameters involving flow rate, flow locations and working periodicity and their impacts on the temperature and dissolved oxygen (DO) distributions of water have been largely unclarified, causing extra time and energy consumptions in practice. In this study, a home-built water tank and an aeration pump are used to model the downwelling aeration processes in stratified water. Temporal influences of aeration parameters on the water stratifications and eutrophicated elements are systemically investigated, with the purpose of searching parametric configurations to enhance the anti-eutrophication efficiency. It is found that the variation rates of temperature destratification and DO distribution in the water body could be saturated and strongly correlated with the flow rate. Based on such experimental saturation rates, we find an optimized working condition from the aspect of energy saving: a 300 rpm pump speed and a 15 cm distance between the flow exit and the sediment surface. In such conditions, the total nitrogen and phosphorus dissolved in the bottom layer of water decrease exponentially with aeration time, and can be reduced by 53.8 and 86% in the first 6 h of aerations, respectively, taking full advantage of the microbial bonding to the sedimentations. The present work provides better understandings for efficient implementations of downwelling aerations.

Keywords Downwelling aeration · Stratified water · Dissolved oxygen · Total nitrogen · Total phosphorus

Introduction

Oceans and lakes are natural carbon sinks, which capture up to 50% of carbon dioxide (CO_2) emitted into the atmosphere through the photosynthesis effect of the aquatic plants, plankton, corals, algae and other photosynthetic bacteria (Yang et al. 2022; Michaelides 2021). However, with the development of industrial farming and urbanization, hypoxia or more severe eutrophication becomes a severe problem for the water quality all over the world (Paerl et al. 2014; Fetahi 2019; Kroeze et al. 2013). Overnourished water body including sharply increasing dissolved nitrogen and phosphorous (Li et al. 2020; Lu et al. 2020), which causes the harmful algae blooms, dissolved oxygen (DO) depletions and dead zones of aquatic life, blocking the mass absorption of CO_2 in the carbon cycle (Pan et al. 2015). Also, the thermal stratification induced by the water density differences further blocks the oxygen diffusion into the deeper regions and releases the pollutants from sediments, aggravating the water quality deterioration (Wells 2020). The polluted water bodies turn out to be carbon sources in these situations.

Since then, people start to seek proper solutions to tackle the eutrophication by using the artificial pumping, which helps the balances of carbons and oxygen in such ecosystems. Among these, downwelling aeration has been proved to be an effective, reliable and economic solution for destratifications hypoxia alleviations (Lu et al. 2020; Koweek et al.

✉ Jiyong Wang
jiyongwang@hdu.edu.cn

1 School of Mechanical Engineering, Hangzhou Dianzi University, Hangzhou 310018, China

2 International Co-Operattion Platform of Intelligent Ocean Equipments Technology of Zhejiang Province, Hangzhou 310018, China

3 Hangzhou Eco-Environment Monitoring Center, 4 Hangda Road, Hangzhou 310000, China

4 School of Electronics and Information, Hangzhou Dianzi University, Hangzhou 310018, China

5 Department of Mechanical and Structural Engineering and Materials Science, University of Stavanger, 4036 Stavanger, Norway

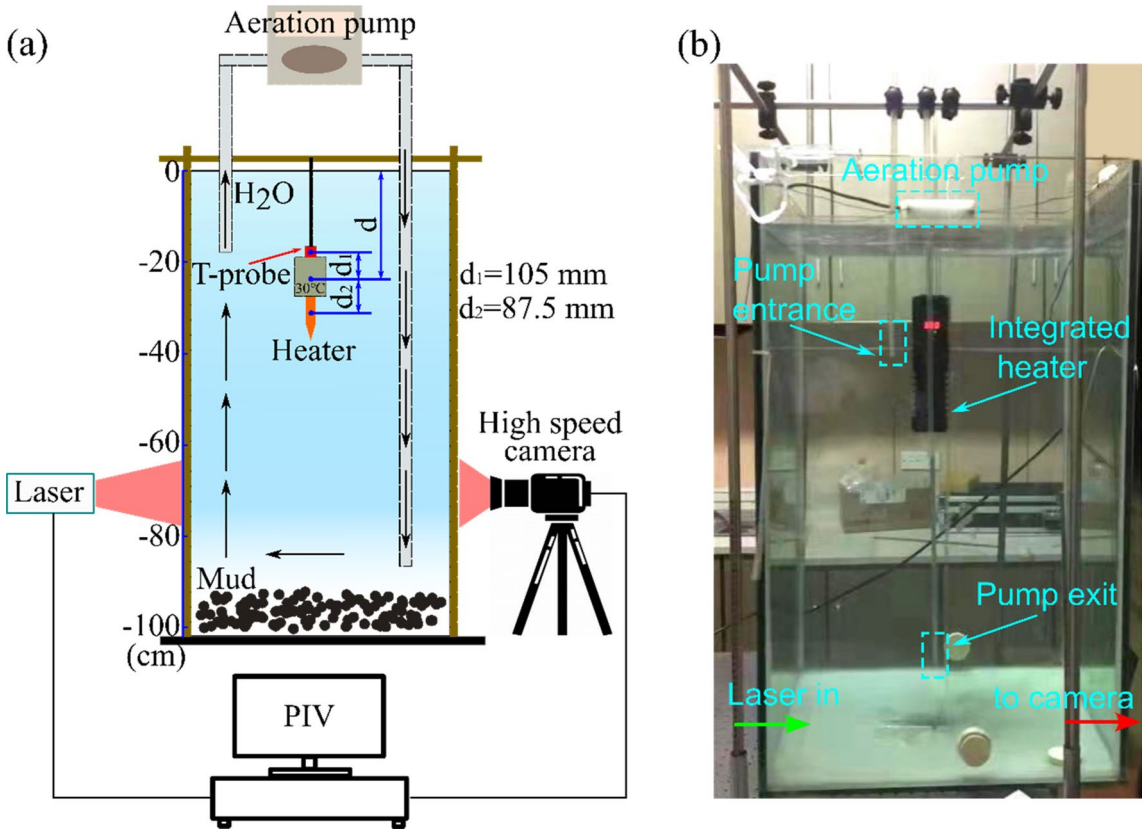

Fig. 1 Experimental setups of downwelling aerations. **a** Illustration and **b** photograph of an artificially pumped aeration platform. PIV denotes Particle Image Velocimetry measurement system. T-probe represents temperature probe. *d*1(*d*2) represents the geometric central distance between the T-probe (heating rod) and the integrated heater. The green and red arrows in **b** represent the incident laser beam and scattered light to the high-speed camera

2020; Roy et al. 2022). There are plenty of studies showing that the global DO levels can be dramatically boosted using downwelling aeration (Roy et al. 2021; Lawson 1995; Bullon et al. 2009; Stigebrandt and Liljebladh 2010). In the meantime, the excess nutrients could be further bounded in the sediments surfaces through chemical reactions (Søndergaard et al. 2003). For example, the dissolved phosphorous could react with anaerobic iron ions in the sediments forming Iron phosphide (Koweek et al. 2020; Hosomi et al. 1982; Tian et al. 2017).

Being one of the most promising artificial pumps, downwelling aerations have been widely applied in practice to increase the DO level in hypolimnion layer of water body, due to a relative high energy efficiency (Koweek et al. 2020; Salter 2009; Antonini et al. 2016; Xiao et al. 2018). However, a quantitative point of view from the aspect of engineering parameters to implement downwelling aerations is still far beyond explored. For example, Stigebrandt and Liljebladh (2010) put the outlets of downwelling pipe ~ 10 m above the sediment top surface in Byfjorden fjord. A relatively high flow rate of water from the pump was employed ~ 4 m^3/s. Fan et al. (2019) designed a tide-powered downwelling pumping device, in which the pipe exit was 0.2 m above the bottom of water body and the flow rate was ~ 0.36 m^3/s. Koweek et al. (2020) located the downwelling pipe exit 0.5 m above the sediment–water interface, the flow rate of which was only ~ 0.03 m^3/s. This configuration required an energy consumption of 0.4 ~ 4 MW/km^3. In general, the aeration parameters for downwelling pumping are quite different from various studies, and their temporal influences on the stratification and oxygenation with consecutive pumping are barely reported. In this study, we experimentally investigate different important aeration parameters including the flow rate, locations of the flow exit, and their influences on the temperature and DO distributions in a finite stratified water volume. The optimized operations of this tank in equilibrium states are proposed for the concern of working efficiency.

Materials and methods

In order to study the temperature stratification of the water and mimic the situation of real lakes, a comprehensive experimental platform is built. As it is shown in Figs. 1a, b,

the whole system mainly consists of a water tank, a velocity recording system and a temperature measurement system. A 600 × 600 × 1000 mm organic glass water tank is built as the experimental water tank. In order to achieve the similar effect of real lake water temperature stratification, an integrated heater combining a heating rod, a digital display and a temperature probe (T-probe) is used to heat the water column and detect the real-time temperature during the experiments. The overall geometry of the integrated heater is 60 × 30 × 270 mm. The distance between the geometric centers of heating rod and temperature sensor is 192.5 mm ($d1 + d2$). For convenience, the geometric center of the heater is used to indicate the depth of the heating source (d). The temperature adjustment range of the heating rod is 20–34 °C where a positive temperature coefficient (PTC) ceramic heating material is used as the heating element. The temperature probe/sensor is made of platinum resistance (Youkesi, PT100) and placed at the top of the heater.

To measure the temperature and DO distributions in the water column, an acrylic board with 10 × 10 through holes is used to hold horizontal positions of T-probe and DO-probe (Lohand Biological, LH-D701, 20 cm length, 1 cm diameter). The through holes are uniformly distributed and the interval between any two adjacent holes is 5 mm. The vertical position of acrylic board is controlled with a "H"-shaped movable frame, which is provided with grooves of 5 cm spacing distance. Thus, 10 × 10 × 14 grids in the water column are generated for temperature and DO measurements.

A particle image velocimetry (PIV) system (Trust Science Innovation, Insight V3V 4G) is used to measure the velocity of water in the experimental tank. The whole system is equipped with a laser (532 nm, 5 ns), a high-speed camera, a synchronizer and a host computer. To measure the water velocity, hollow glass spheres (14–17 μm) are mixed with water and illuminated by the expanded laser beam. The scattered light from hollow spheres is detected by high-speed camera in a vertical image plane of 70 × 70 cm. The velocity is calculated by tracing the movement of hollow spheres in water.

The sediment mud and water bodies from a lightly polluted river (Yueya river, Hangzhou, China, date: August 3, 2021) are used as the investigated objects. The thickness of sedimentation mud is 20 cm and the depth of the water column is 70 cm. The bottom water is collected with a home-built liquid sampler at every 6 h from approximately 1 cm above the top surface of sediments to measure the concentration of total phosphorus (TP) and total nitrogen (TN). All the collection and measurement of TN and TP are conducted in accordance with the Chinese government standards (HJ636-2012 and HJ671-2013). For the TN measurement, the key operating procedures follow: (1) take 10 ml of water sample and 5 ml potassium persulfate solution into a 25 ml grinding glass colorimetric tube with plug; (2) heat the closed colorimetric tube in a high-pressure steam sterilizer in a temperature 120 °C for 30 min and cool it to room temperature in air; (3) add 1 ml concentrated hydrochloric acid (ρ(HCl) = 1.19 g/ml) and use water to dilute to 25 ml; (4) measure the absorbance of the above solution using UV spectrophotometer with a 10 mm quartz cuvette at the wavelengths of 220 and 275 nm; (5) calculate the TN concentration in sample (mg/L) in standard UV spectrophotometric method. More details about the measurements can be found from Chinese government standard HJ636-2012. For each measurement of TN concentration, we repeat three times and take the averaged value.

For the TP measurement, 100 ml water sample and the following key reagents are arranged in a continuous flow injection analyzer (Netherland, SKALAR San++) to mix and react in a specific order and ratio, and enter the flow detection cell for photometric detections: (1) sulfuric acid, $\rho = 1.84$ g/ml, 95–98%; (2) potassium peroxodisulfate, $K_2S_2O_8$; (3) ammonium heptamolybdate tetrahydrate, $(NH_4)_6Mo_7O_{24}{\cdot}4H_2O$; (4) antimony potassium tartrate trihydrate, $K_2(SbO)_2C_8H_4O_{10}{\cdot}3H_2O$; (5) sodium dodecyl sulfate, $NaC_{12}H_{25}SO_4$; (5) potassium dihydrogen phosphate, KH_2PO_4, dried at 105 ± 5 °C to constant mass; (6) potassium pyrophosphate, $K_4P_2O_7$; (7) pyridoxal-5-phosphate monohydrate, $C_8H_{10}NO_6P{\cdot}H_2O$; (8) disodium phenylphosphate, $C_6H_5Na_2PO_4$. More details about the measurements can be found from Chinese government standard HJ671-2013. For each measurement of TP concentration, we repeat three times and take the averaged value.

A peristaltic pump (Runze Fluid, LM50) is used to exchange the water from different layers of water tank. Two plastic pipes (outside diameter: 11 mm, inside diameter: 8 mm) are connected with the entrance and the exit of the pump. When the pump rotates in a speed of 100, 200, 300 and 400 rpm, the flow velocity in pipes is measured by PIV, which is 0.0995, 0.2089, 0.3382, and 0.4178 m/s, respectively.

Results and discussions

Water stratification

In order to explore the influence of artificial heater on the water stratification, the heating rod with different initial temperatures is placed in different depths of water column. Figure 2 shows the water stratifications impacted by the temperature and the depth of the heat source. In Fig. 2a, the initial temperature of heating rod is set to 25 °C (red), 30 °C (green) and 34 °C (blue). The vertical distance (d) between the geometric center of heater and the water surface is 30 cm. After continuous heating for 10 h in each case, the

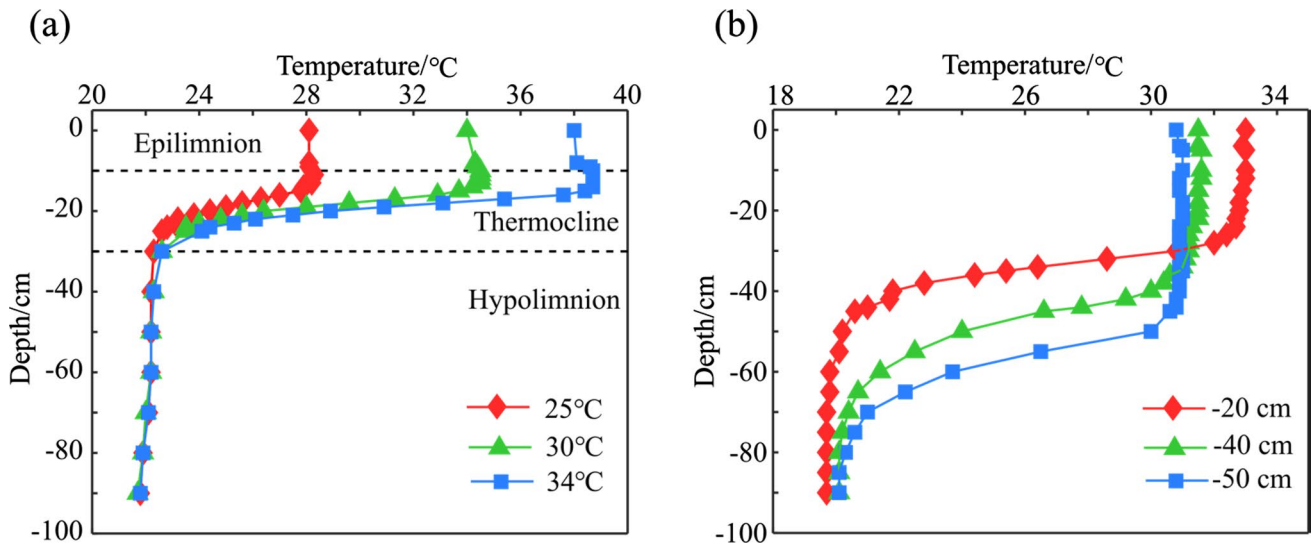

Fig. 2 Water stratification impacted by the temperature (**a**) and the depth (**b**) of the heat source

temperature distribution of water column is measured and shown in Fig. 2a.

It can be seen that no matter to what magnitude the temperature of heating rod is set, the position of each layer of the water column remains almost unchanged. The boundary between the epilimnion and the thermocline is found to be 15 cm below the water surface. The boundary between the thermocline and the constant temperature layer is 30 cm below the water surface. The temperature of the constant temperature layer is maintained at around 22 °C. As the surface temperature increases, the average temperature of the thermocline rises. The temperature of epilimnion changes from 28, 34 to 38 °C for the heater temperature of 25, 30 and 34 °C, respectively. For the three different heating rod temperatures, the temperature of the water column at the boundary between hypolimnion and thermocline, that is 30 cm below water surface, are 22.3, 22.6 and 22.6 °C, respectively. The temperature of the water column at the depth of 40 cm reaches 22 °C for the cases of three difference temperatures of the heater. Apparently, the thermocline appears with certain temperature gradients and this region can be recognized with two turning points (inflection), as shown in Fig. 2a. The temperature in this regime declines rapidly with the depth. The density changing at the thermocline acts as a physical barrier, preventing the mixing of the upper and lower layers (Wetzel 2001).

On the other hand, it can also be found that the water column temperature at the top of the heater (at 19.5 cm below the water surface) can reach the setting values at the equilibrium state. The density of water column is changing during the heating process. A relatively stable upward flow is formed in the water tank which makes the water on the top of the heating rod form a high temperature area. The highest temperatures are 12.8, 15 and 13.8% higher than those of the setting temperatures. On average, the surface temperature of thermosphere is 13.45% higher than the setting temperature.

In order to simulate the water stratification of the real lakes, we further explore the effect of heating depth. The depth of the geometric center of the heater (d) is moved from 20, 40m to 50 cm consecutively away from the water surface, and the target temperature of heating rod is set to 33 °C. After 10 h of continuous heating in each case, the temperature distribution of water column is shown in Fig. 2b. It can be seen that as the depth increases, the position of water stratification (especially thermocline layer) gradually moves downward. The thickness of epilimnion increases linearly and hypolimnion layer thickness decreases. In the following experiments of sections "Influence of aeration speed on stratified temperature and dissolved oxygen" and "Influence of aeration on sediments", we choose the heating depth of 20 cm, as the normalized layer structure of the stratified water is similar to actual lakes in South China (Zhang et al. 2015; Liu et al. 2019; Yang et al. 2020).

Influence of aeration speed on stratified temperature and dissolved oxygen

As the stratification of the water column is stabilized, a pump is further used for transferring water from the epilimnion through the thermocline to the hypolimnion. The rotation speed of downwelling pump is set consecutively to 100 rpm (flow rate 0.3 L/min), 200 rpm (flow rate 0.63 L/min), 300 rpm (flow rate 1.02 L/min) and 400 rpm (flow rate 1.26 L/min), respectively. The flow exit is 10 cm above the sediment surface. The state of water temperature stratification is studied at each time period. The temperature is

measured every 2 h. Figure 3 shows the influence of aeration speeds on the temporal thermal stratification. When the rotation speed is 100 rpm, the water temperature changes with the depth, as shown in Fig. 3a. The stratification is, however, barely affected by the aeration in the first 14 working hours. Nevertheless, when the rotation speed is increased to 200 rpm (Fig. 3b), 300 rpm (Fig. 3c) and 400 rpm (Fig. 3d), distinct pictures are observed. Firstly, as it can be observed from Figs. 3b, d, with increasing working time of the aeration pump, the temperature of water column in the constant temperature (Isothermal hypolimnion) layer gradually increases, basically showing functionally a logarithmic changing trend until it approaches the surface temperature of the water column. Secondly, it is clearly seen that with the flow rate increasing, the destratification time is dramatically reduced. We take the boundary between the epilimnion and thermocline for example. The criterion to determine such a boundary is based on a difference of 5% from the average temperature of epilimnion layer. It is clearly observed that the boundary disappears after a continuous aeration of 5.5 and 3.2 h for the rotation speed of 200 and 300 rpm, respectively, indicating the ambiguous role of the aeration on the destratification. However, it is also observed that with further increase in the pumping speed, the destratification rate will not increase. Figure 3d shows that the boundary disappears after approximately 3.2 h continuous aeration.

The pump pushes oxygenated surface water downward inducing downwelling to increase the oxygen levels of the water underneath. Downwelling is thus recognized as a promising technique for treating coastal pollution, owing to its potential to passively harness the hypoxia (Roy et al. 2021). In order to study the influence of aeration on the

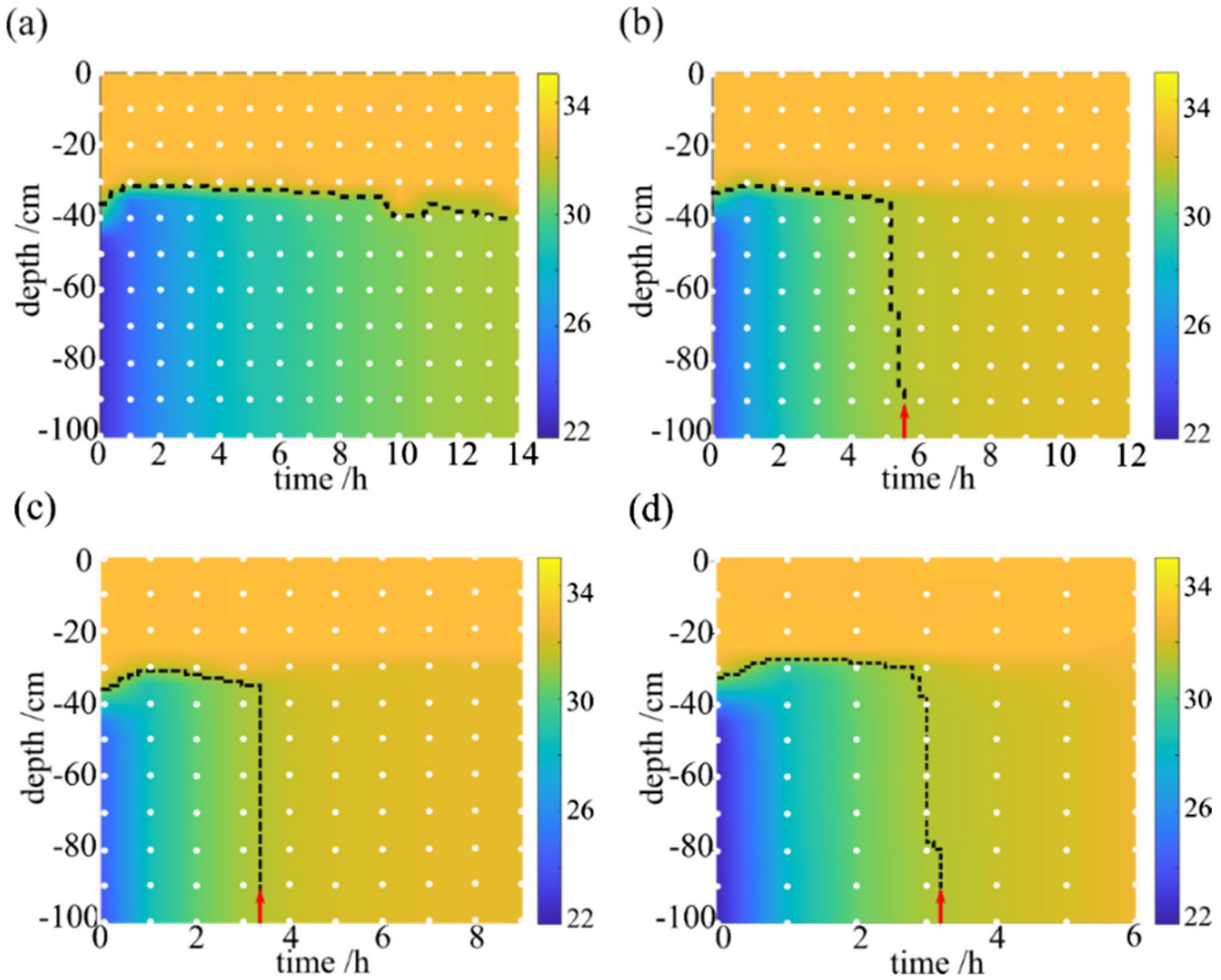

Fig. 3 Influence of aeration speed on the temporal thermal stratification. The rotation speed of the pump ranges from 100 rpm (**a**), 200 rpm (**b**), 300 rpm (**c**) to 400 rpm (**d**). The dashed black lines imply the boundary between the epilimnion and thermocline layers. The red arrows indicate the boundary vanishing time

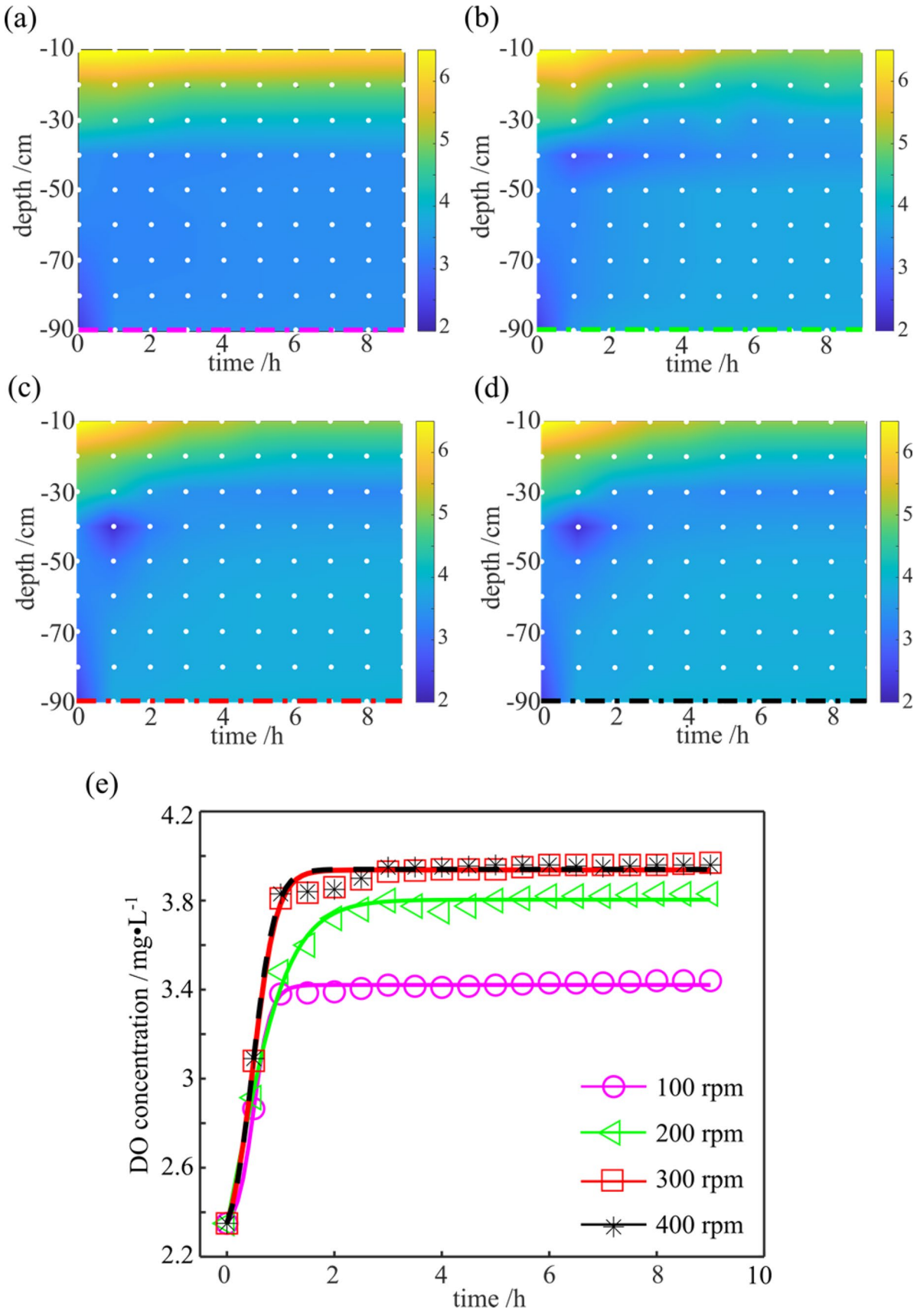
(a)
(b)
(c)
(d)
(e)
depth /cm
time /h
DO concentration / mg•L-1
100 rpm
200 rpm
300 rpm
400 rpm

◂**Fig. 4** Influence of aeration speed on the temporal responses of stratified dissolved oxygen. The rotation speed of the pump ranges from 100 rpm (**a**), 200 rpm (**b**), 300 rpm (**c**) to 400 rpm (**d**). **e** DO concentration at the bottom of the water column (dashed horizontal lines at the bottom of each figure) as functions of aeration time and rotation speed

oxygen, DO in different stratified water bodies at different flow rates is explored with consecutive underwater aeration. A comparative assessment among Figs. 4a–d reveals that the concentration of DO in the water column with a constant temperature layer, gradually increases with the increasing aeration time. When the rotation speed is 100 rpm, as shown in Fig. 4a, DO stratification is obvious in the water column and is close to the saturated value near the water surface. However, when the rotation speed is increased to 200 rpm, after 5 h aeration, the DO concentration is around 5 mg/L at the surface (Fig. 4b), which is much lower than the saturated value. When the rotation speed is further increased to 300 and 400 rpm, the DO concentration in the surface is decreased to 4.5 mg/L after a much shorter aeration time (4 h). Another important observed feature is a global increase in DO level in the hypolimnion with the increasing rotation speed. To obtain a clearer picture, the temporal responses of the DO concentration at the bottom layer of water column (10 cm above the sedimentation) under different rotation speeds are compared. The absolute depths are illustrated by the dashed horizontal lines in Figs. 4a–d. In Fig. 4e, DO rapidly increases in the first 2 h of aeration, and then gradually approaches to a saturated level. With the increase in rotation speed, there is a general increase in rise rate and the saturated level of DO until the rotation speed reaches 300 rpm. It is clearly seen that even the rotation speed is further increased to 400 rpm, the DO concentration has almost the same tendency as the case of 300 rpm rotation speed. This implies that the rotation speed of 300 rpm could be the optimal pumping speed for the concern of energy saving.

Influence of aeration on sediments

In real lakes and rivers, the overlaying water of sedimentation often has a significant impact on the water quality of water column, because of a stronger phosphorous or nitrogen reservation, in comparison with the water in other regions (Hosomi et al. 1982; Gorham and Boyce 1989; Tekile et al. 2017). In order to explore the influence of downwelling aeration on the overlaying water of sedimentations, the flow fields under different aeration depths are experimentally measured using the PIV system. The ambient temperature is 21 °C. The artificial heater is located at 20 cm below the water top surface and is set to 33 °C. The speed of peristaltic pump is set to the optimal value, that is, 300 rpm with a flow rate of 1.02 L/min. Once the peristaltic pump is implemented, the water flow fields around the exit pipe are measured. Figure 5 shows the influence of aeration on sediments in terms of flow fields at different locations above the sedimentation mud layer as well as the time history data of TN and TP concentrations.

For the downwelling aeration, it is a tradeoff to determine a proper vertical location of flow exit. On the one hand, the lowest flow exit is expected to increase the flow circulation length and thus the DO contents. On the other hand, sever disturbances to the bottom sediments should be avoided, so that exceed nutrients bounded to sediments would not be forced to release. Figure 5a–c show that with increasing aeration distance between the flow exit and top surface of the sediments, the smaller the disturbance range is firstly observed. When the distance is 10 cm, the water flow is quite strong due to a high-speed flow core very near the mud. The upside sediments are forced to move, and certain amount of phosphorus and other excess nutrients which is bound to sediments will be diffused to the water body. With an increase in such a distance to 15 cm, the water flow becomes weak. The sediments movement is slowed down, so the nutrient in sediments could be remained stable. The velocity of the central flow at the bottom plane in such a case is around 0.14 m/s, which corresponds to a finite water volume rises a height of 1 mm. When the distance is further increased to 20 cm, the flow circulation length becomes much shorter than the case of 15 cm, although a much weaker disturbance to the bottom sediments could be expected. Thus, to avoid the release of excess nutrients in the sediments as well as achieve long circulation flows, an optimal distance between the flow exit and the overlaid sediments should be seeked. In our modeling system, a 15 cm distance could be optimal among the three depth options.

To study the effect of aeration on bottom water quality and biological activity, the changes of TN and TP concentrations in overlaying water are measured. A 300 rpm speed of aeration pump and a 15 cm distance between the flow exit and the top surface of the sediments are used for a consecutive aeration of 192 h. In Fig. 5d, the concentrations of both TN and TP in the bottom water decreases exponentially with the aeration time. It decreases dramatically at the first 6 h and remains almost the same level after that. At the initial stage, the dissolved nutrients are interchanged between different layers and partially bound to the bottom sediments through aerations. With the progress of aeration, although the DO concentration in the bottom water increases, bacteria cannot consume all the nutrient elements. The TP and TN concentrations in the water column finally approach their equilibrium states. The decay rates can be obtained by fitting the experimental data, which are 1.35 mg/(L h) and 1.76 mg/(L h) for the TN and TP concentrations, respectively.

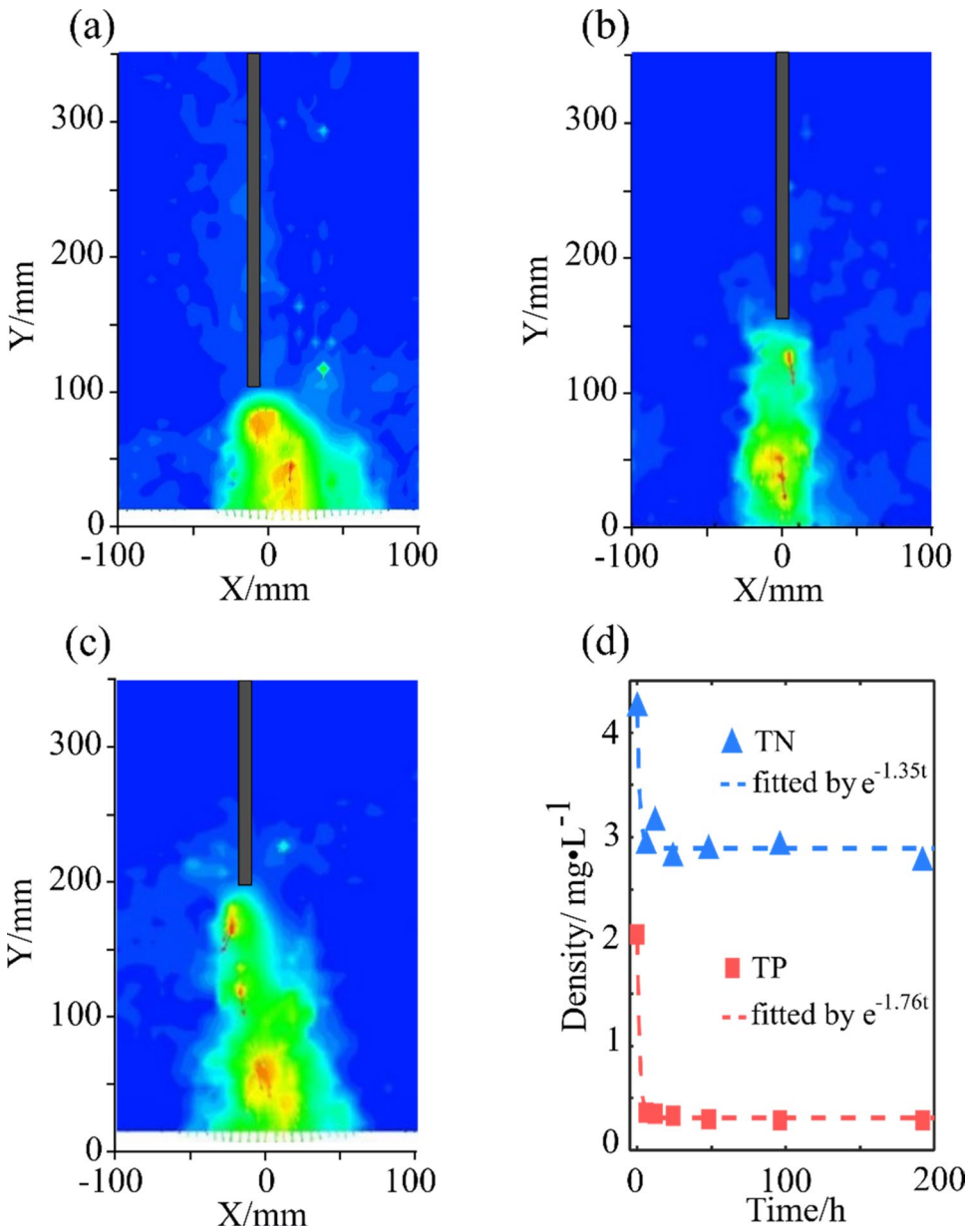

Fig. 5 Influence of aeration on sediments. (a)-(c) flow fields of the pump exit locating at 100 mm (**a**), 150 mm (**b**) and 200 mm (**c**) above the sedimentation mud layer. The location Y = 0 indicates the top surface of the sediments. The rotation speed is chosen as 300 rpm. **d** The concentrations of TN (blue triangles) and TP (red squares) as functions of aeration time. The dashed lines are the fitted exponential functions with a decay rate of 1.35 (red dashed line) and 1.76 (blue dashed line) for TN and TP concentrations, respectively

Finally, we discuss about the working periodicity of the aeration pump, taking both the environmental parameters (thermal stratification, DO, TN and TP) and the energy consumption into account. Depending on the pollution level, different strategies on working periodicity should be employed. For heavily polluted waters, at least 6 h of consecutive pumping is required for each aeration period, in order to better depress the general level of dissolved TN and TP in the water body, as shown in Fig. 5d. In such 6 h of pumping, the thermal destratification and DO saturation are simultaneously achieved, which can be clearly observed from Figs. 3c and 4e. However, for mild polluted waters, it is possible to promote the DO level without destroying natural stratifications, which is important to maintain the vertical biodiversity of a water ecosystem (Ullyott and Holmes 1936; Boehrer and Schultze 2008). The on-pumping time in each aeration period could be reduced to around 2 h, if only stratification maintenance and DO saturation are considered. It is still possible to suppress the TN and TP concentrations to a proper level in one period of 2 h. However, to reduce the TN and TP to their minimal levels, as shown in Fig. 5d, it might take several aeration periods. The off-pumping time becomes another key factor to be determined, as the environmental parameters tend to restore to their original levels. This might need combine diffusion theories of multiple physics with the optimization algorithms in mathematics, in order to find an optimal balance between the environmental parameters and the energy used.

For future work, more specific experiments are expected to conduct from the following aspects: a) Experimental study on the pumping periodicity, off-pumping time in particular, taking both the energy consumption and the nutrient reduction into account; b) Adaptions and corrections of the current model system to a real scenario.

Conclusions

A home-built water tank and the sediments from a mild polluted lake are used to model the aeration impacts on the water environment in the present study. An artificial heat source is firstly applied to form similar thermal stratifications to the real lakes by altering the source temperature and locations. The temporal temperature and DO distributions under different flow rates are then experimentally measured. It is found that the optimal aeration rotation speed is around 300 rpm, at which the destratification time is shortest and the saturated DO level reaches its maxima. The flow fields at the vicinity of pipe exit are measured using PIV system. The optimal location of the flow exit is tested, where the minimum perturbation is aroused to the sediment layer and the maximum flow circulation is achieved. By using the optimized hypodynamic control parameters (300 rpm, 15 cm away from the sediment surface), the TN and TP concentrations in the overlaying water of the sediments are recorded in a 192-h consecutive aeration. The present result shows that the TN and TP could be reduced by 53.8% and 86% in the first 6 h of aerations, respectively. Further considerations for an effective periodic aeration in real situations are discussed in the end. The study provides a practical guide for downwelling aeration implementations, and certain perspectives on nutrient reduction measures.

Funding This work was supported by the National Natural Science Foundation of China (No. 51709070), Key R&D Program of Zhejiang Province (No. 2021C03013), and the Fundamental Research Funds for the Provincial Universities of Zhejiang (No. GK229909299001-007). The funders had no role in study design, data collection and analysis, decision to publish, or preparation of the manuscript.

Data availability The data presented in this study are available on request from the corresponding author.

Declarations

Conflicts of interest The authors declare no conflict of interest.

References

Antonini A, Lamberti A, Archetti R et al (2016) CFD investigations of OXYFLUX device, an innovative wave pump technology for artificial downwelling of surface water. Appl Ocean Res 6:16–31

Boehrer B, Schultze M (2008) Stratification of lakes. Rev Geophys 46:RG2005

Bullon P, Morillo JM, Ramirez-Tortosa MC et al (2009) Metabolic syndrome and periodontitis: is oxidative stress a common link? J Dent Res 88:503–518

Fan W, Pan D, Xiao C et al (2019) Experimental study on the performance of an innovative tide-induced device for artificial downwelling. Sustainability 11:5268

Fetahi T (2019) Eutrophication of Ethiopian water bodies: a serious threat to water quality, biodiversity and public health. Afr J Aquat Sci 44:303–312

Gorham E, Boyce FM (1989) Influence of lake surface area and depth upon thermal stratification and the depth of the thermocline. J Great Lakes Res 15:233–245

Hosomi M, Okada M, Sudo R (1982) Release of phosphorus from lake sediments. Environ Int 7:93–98

Koweek DA, Garcia-Sanchez C, Brodrick PG et al (2020) Evaluating hypoxia alleviation through induced down-welling. Sci Total Environ 719:137334

Kroeze C, Hofstra N, Ivens W et al (2013) The links between global carbon, water and nutrient cycles in an urbanizing world—the case of coastal eutrophication. Curr Opin Environ Sustain 5:566–572

Lawson TB (1995) Oxygen and aeration. fundamentals of aquacultural engineering, 1st edn. Springer, Boston, pp 248–310

Li Z, Zhang R, Liu C et al (2020) Phosphorus spatial distribution and pollution risk assessment in agriculture soil around the Danjiangkou reservoir. China Sci Total Environ 699:140958

Liu M, Zhang Y, Shi K et al (2019) Thermal stratification dynamics in a large and deep subtropical reservoir revealed by high frequency buoy data. Sci Total Environ 651:614–625

Lu C, Cheng W, Wang M et al (2020) Combining artificial aeration and biological zeolite mulch for nitrogen removal from eutrophic water bodies. Water Pract Technol 15:151–159

Michaelides EE (2021) Thermodynamic analysis and power requirements of CO_2 capture, transportation, and storage in the ocean. Energy 230:120804

Paerl HW, Gardner WS, Mccarthy MJ et al (2014) Algal blooms: noteworthy nitrogen. Science 346:175–176

Pan Y, Fan W, Huang TH et al (2015) Evaluation of the sinks and sources of atmospheric CO_2 by artificial upwelling. Sci Total Environ 511:692–702

Roy SM, Tanveer M, Machavaram R (2021) Applications of gravity aeration system in aquaculture-a systematic review. Aquac Int 30:1593–1621

Roy SM, Machavaram R, Moulick S et al (2022) Economic feasibility study of aeration in aquaculture using life cycle costing (LCC) approach. J Environ Manag 302:114037

Salter S (2009) Wave-powered destratification for hurricane suppression, acidity reduction, carbon storage and enhanced phytoplankton, dimethyl sulphide and fish production. In: IOP conference series earth and environmental science, Copenhagen, Denmark

Søndergaard M, Jensen JP, Jeppesen E (2003) Role of sediment and internal loading of phosphorus in shallow lakes. Hydrobiologia 506:135–145

Stigebrandt A, Liljebladh B (2010) Oxygenation of large volumes of natural waters by geo-engineering: with particular reference to a pilot experiment in Byfjorden. Macro-engineering seawater in unique environments, 1st edn. Springer, Berlin, pp 303–315

Tekile A, Kim I, Lee JY (2017) Field study of water quality improvement by circulation, sonication and ozonation. J Korean Soc Water Environ 33:170–180

Tian X, Pan H, Kongas P et al (2017) 3D-modelling of the thermal circumstances of a lake under artificial aeration. Appl Water Sci 7:4169–4176

Ullyott P, Holmes P (1936) Thermal stratification in lakes. Nature 138:971

Wells SA (2020) Modeling thermal stratification effects in lakes and reservoirs. In: Inland waters-dynamics and ecology, 1st edn. IntechOpen, London

Wetzel RG (2001) Limnology lake and river ecosystems, 3rd edn. Academic Press, San Diego

Xiao C, Fan W, Qiang Y et al (2018) A tidal pump for artificial downwelling: theory and experiment. Ocean Eng 151:93–104

Yang X, Li Y, Wang B et al (2020) Effect of hydraulic load on thermal stratification in karst cascade hydropower reservoirs, Southwest China. J Hydrol: Reg Stud 32:100748

Yang J, Han M, Zhao Z et al (2022) Positive priming effects induced by allochthonous and autochthonous organic matter input in the lake sediments with different salinity. Geophys Res Lett 49:e2021GL096133

Zhang Y, Wu Z, Liu M et al (2015) Dissolved oxygen stratification and response to thermal structure and long-term climate change in a large and deep subtropical reservoir (Lake Qiandaohu, China). Water Resour 75:249–258